# Changes in the Structure of Calmodulin Induced by a Peptide Based on the Calmodulin-Binding Domain of Myosin Light Chain Kinase†

D. B. Heidorn,‡ P. A. Seeger,§ S. E. Rokop,‡ D. K. Blumenthal,‖ A. R. Means,⊥ H. Crespi,# and J. Trewhella*,‡,§

*Life Sciences Division and Neutron Scattering Center, Los Alamos National Laboratory, Los Alamos, New Mexico 87545, Department of Biochemistry, University of Texas Health Center at Tyler, Tyler, Texas 75710, Department of Cell Biology, Baylor College of Medicine, Houston, Texas 77030, and Chemistry Division, Argonne National Laboratory, Argonne, Illinois 60439*

*Received March 21, 1989; Revised Manuscript Received May 2, 1989*

ABSTRACT: Small-angle X-ray and neutron scattering data were used to study the solution structure of calmodulin complexed with a synthetic peptide corresponding to residues 577–603 of rabbit skeletal muscle myosin light chain kinase. The X-ray data indicate that, in the presence of $Ca^{2+}$, the calmodulin–peptide complex has a structure that is considerably more compact than uncomplexed calmodulin. The radius of gyration, $R_g$, for the complex is approximately 20% smaller than that of uncomplexed $Ca^{2+}$·calmodulin (16 vs 21 Å), and the maximum dimension, $d_{max}$, for the complex is also about 20% smaller (49 vs 67 Å). The peptide-induced conformational rearrangement of calmodulin is [$Ca^{2+}$] dependent. The length distribution function for the complex is more symmetric than that for uncomplexed $Ca^{2+}$·calmodulin, indicating that more of the mass is distributed toward the center of mass for the complex, compared with the dumbell-shaped $Ca^{2+}$·calmodulin. The solvent contrast dependence of $R_g$ for neutron scattering indicates that the peptide is located more toward the center of the complex, while the calmodulin is located more peripherally, and that the centers of mass of the calmodulin and the peptide are not coincident. The scattering data support the hypothesis that the interconnecting helix region observed in the crystal structure for calmodulin is quite flexible in solution, allowing the two lobes of calmodulin to form close contacts on binding the peptide. This flexibility of the central helix may play a critical role in activating target enzymes such as myosin light chain kinase.

A variety of eukaryotic processes, including muscle contraction, cell division, cyclic nucleotide metabolism, and glycogen metabolism, are regulated by changes in the intracellular concentration of $Ca^{2+}$. A large number of these processes are known to be mediated by the $Ca^{2+}$-binding protein calmodulin. The structure of calmodulin exhibits a number of unusual features that appear to be related to its ability to regulate a diverse array of target proteins in a variety of eukaryotic cells. The primary structure of calmodulin, which has been highly conserved throughout eukaryotic evolution, contains four homologous helix–loop–helix structures that function to bind $Ca^{2+}$ [reviewed by Wylie and Vanaman (1988)]. These four $Ca^{2+}$-binding domains are arranged as two globular lobes, each lobe containing two $Ca^{2+}$-binding domains. The two lobes are connected by a single seven-turn, solvent-exposed $\alpha$-helix (Babu et al., 1985). The crystallographic temperature factors for residues in this central helix indicate it is a region of greater conformational flexibility compared with the rest of the structure (Babu et al., 1988). There is further evidence that indicates this central helix is quite flexible in solution and may have an important function as a tether (Persechini & Kretsinger, 1988; Heidorn & Trewhella, 1988; Putkey et al., 1988; Persechini et al., 1989). Upon binding $Ca^{2+}$, calmodulin undergoes a number of structural changes including the exposure of a hydrophobic cleft in each globular lobe. It is thought that hydrophobic interactions involving these two nonpolar regions may be important in calmodulin–target enzyme interactions (LaPorte et al., 1980; Tanaka & Hidaka, 1980; Babu et al., 1988).

Although a great deal is known at the molecular level about the structural changes occurring in calmodulin as a result of binding $Ca^{2+}$, much less is known about the molecular interactions of calmodulin with its various target proteins. This is primarily due to practical limitations such as the prohibitively large quantities of protein required for many physical studies and the difficulty in interpreting the complex patterns of data obtained because of the high molecular weights of most target enzymes. However, a number of calmodulin-binding proteins have recently been sequenced and their putative calmodulin binding domains identified. In several instances, synthetic peptides based on the sequences of these domains have been prepared and have been shown to bind calmodulin in a $Ca^{2+}$-dependent manner with the same stoichiometry and affinity as the native protein (Blumenthal & Krebs, 1988; Hanley et al., 1987; Kemp et al., 1987; Payne et al., 1988). These synthetic calmodulin-binding domain peptides are now being widely used as models to study the molecular details of calmodulin–target enzyme interactions.

Myosin light chain kinase (MLCK)[1] from rabbit skeletal

† This work was performed under the auspices of the DOE (Contract W-7405-ENG-36) and is supported by NIH Grants GM40528 (J.T.), GM39290 (D.K.B.), and GM33976 (A.R.M.) and by DOE/OHER Project HA-02-02-03/B04664 (J.T.). This work has benefited from the use of facilities at the Los Alamos Neutron Scattering Center, a national user facility funded as such by the DOE/Office of Basic Energy Sciences.

* Address correspondence to this author at the Life Sciences Division, Los Alamos National Laboratory.

‡ Life Sciences Division, Los Alamos National Laboratory.

§ Neutron Scattering Center, Los Alamos National Laboratory.

‖ University of Texas Health Center at Tyler.

⊥ Baylor College of Medicine.

# Argonne National Laboratory.

0006-2960/89/0428-6757$01.50/0 © 1989 American Chemical Society

muscle is a well-characterized calmodulin-dependent enzyme. The enzyme catalyzes the phosphorylation of the P-light chain subunit of myosin which has been proposed to give rise to the contractile phenomenon known as posttetanic twitch potentiation [reviewed by Stull (1988)]. The calmodulin-binding domain of skeletal muscle MLCK was the first such domain to be identified, and synthetic peptides based on its sequence have been used in several spectroscopic and biochemical studies of calmodulin–MLCK interactions (Blumenthal et al., 1985; Klevit et al., 1985; Klevit & Blumenthal, 1987; Persechini et al., 1989; Nunnally et al., 1987). The minimal essential sequence for binding calmodulin with high affinity corresponds to residues 577–593 of MLCK (Blumenthal & Krebs, 1988), although most studies to date have employed a 26-residue peptide (referred to as M13 or MLCK-I) corresponding to residues 577–603. The synthetic MLCK calmodulin-binding peptides bind calmodulin with high affinity ($K_d \sim 1$ nM) and a 1/1 stoichiometry and have been shown to inhibit competitively the calmodulin-dependent activation of MLCK (Blumenthal et al., 1985). Data from circular dichroism (CD) studies indicate that the MLCK peptide assumes an $\alpha$-helical conformation upon binding calmodulin (Klevit et al., 1985), which is consistent with the predicted $\alpha$-helical propensity of the peptide's sequence. Proton NMR spectroscopic studies indicate that calmodulin also undergoes global structural changes upon forming a complex with the MLCK peptide (Klevit et al., 1985; Klevit & Blumenthal, 1987).

Although it is clear that major structural changes in calmodulin and the MLCK peptide occur upon binding, details of the final structures of the two molecules in the complex are as yet unknown. Because information concerning the disposition of the MLCK peptide and calmodulin in the complex may contribute to our understanding of the interactions of MLCK as well as other target proteins with calmodulin, we have undertaken the studies reported here. The combined use of small-angle X-ray and small-angle neutron scattering using deuterated calmodulin provides insights into the overall solution structure of the complex which are inaccessible by other methods. Application of these techniques to other peptides and eventually to larger fragments of, or possibly intact, target enzymes promises to provide data that will further our understanding of the regulation of calmodulin-dependent processes at the molecular level.

## Materials and Methods

*Peptide and Protein Preparation.* The MLCK-I peptide having the sequence Lys-Arg-Arg-Trp-Lys-Lys-Asn-Phe-Ile-Ala-Val-Ser-Ala-Ala-Asn-Arg-Phe-Lys-Lys-Ile-Ser-Ser-Ser-Gly-Ala-Leu-$NH_2$ was synthesized, purified, and characterized as described previously (Blumenthal & Krebs, 1987), except that a Biosearch SAM II automated peptide synthesizer was used together with minor modifications in the synthesis protocol. A benzhydrylamine resin (Peninsula Labs) was used as a solid support, and BOC-Asn was used without side-chain protection as recommended by Biosearch. To minimize side reactions, 1.5 equiv of 1-hydroxybenzotriazole was added during Asn couplings.

Bovine calmodulin (b-CaM) was purchased from Calbiochem and used without further purification. Bacterially synthesized calmodulin (c-CaM, for "cloned" CaM) was purified from *Escherichia coli* N5151 or AR68 containing the plasmid pCam23PL (Putkey et al., 1986). Fractions containing c-CAM from the phenyl-Sepharose column were combined and brought to 1.5 mM $CaCl_2$. This solution was concentrated to approximately 0.5 mL by using a 5000 molecular weight cutoff filter in an Amicon ultrafiltration cell. The c-CaM solution was further purified by chromatography on a 90 × 1.5 cm Sephadex G50 superfine column using a buffer containing 50 mM Tris, pH 7.5, 1 mM $CaCl_2$, and 100 mM KCl. The combined peak fractions were assayed for purity by using SDS gel electrophoresis and X-ray scattering. A pure c-CaM sample gave values for the X-ray forward scattering intensity and $R_g$ consistent with the known molecular weight and dimensions of the protein (Heidorn & Trewhella, 1988). It was sometimes necessary to rechromatograph the c-CaM on the final Sephadex G50 SF column in order to obtain a sample that gave a gel pattern and X-ray scattering parameters characteristic of pure calmodulin. Deuterated c-CaM was prepared by the same protocol using cells adapted to grow in 99.9% $^2H_2O$ on a deuterated substrate as described by Seeholzer et al. (1986). Typical yields were 20–30 mg of pure protein per liter of growth media for proteated (i.e., nondeuterated) c-CaM and 5–10 mg of pure protein per liter for deuterated c-CaM.

Calmodulin samples for scattering experiments were typically prepared by concentrating to a protein concentration of 30–50 mg/mL and dialyzing against several changes each of 100 mM KCl, 1 mM EGTA, and 50 mM MOPS, pH 7.4, buffer and then several changes of 100 mM KCl and 50 mM MOPS, pH 7.4, buffer. For X-ray samples, the appropriate amounts of $CaCl_2$ and/or peptide were then added. Protein and peptide concentrations were determined spectrophotometrically using an extinction coefficient of 0.18 at 277 nm for a 1 mg/mL solution of calmodulin and a molar extinction coefficient of 5550 at 280 nm for MLCK-I. In the case of the deuterated c-CaM, the protein was lyophilized after the above dialysis, weighed, and taken up in the appropriate deuterated buffers containing MLCK-I and/or $Ca^{2+}$. The concentration of deuterated c-CaM was then determined by using the optical absorption at 277 nm; this value was always within 10% of the value determined from weighing. All dilutions were done by weighing. Final samples for scattering measurements were in 50 mM MOPS, pH 7.4, and 100 mM KCl buffer. MLCK-I was always added to calmodulin in a 1/1 stoichiometry, and $Ca^{2+}$-containing samples had 50 mM $CaCl_2$ to ensure that all $Ca^{2+}$-binding sites were filled.

*Scattering Data Acquisition and Reduction.* X-ray data were collected on the small-angle X-ray scattering station at Los Alamos which has been described previously (Heidorn & Trewhella, 1988).

The neutron scattering experiments were carried out on the Low-Q diffractometer (LQD) (Seeger et al., 1986, 1989) at the Los Alamos Neutron Scattering Center (LANSCE). LANSCE provides a spallation source which produces pulses of neutrons with a wide band of wavelengths; the "time of flight" of neutrons from the source to the detector is used to determine the wavelength of each detected neutron with high precision. Data reduction in this experiment differs from a monochromatic source in that all data must be converted to momentum units [$Q = (4\pi \sin \theta)/\lambda$, where $\theta$ is half the

[1] Abbreviations: ATPase, adenosine-5′-triphosphatase; b-CaM, bovine brain calmodulin; c-CaM, cloned calmodulin; $Ca^{2+}$-calmodulin, calmodulin complexed with four $Ca^{2+}$; CD, circular dichroism; $d_{max}$, maximum linear dimension; DTT, dithiothreitol; EDTA, ethylenediaminetetraacetic acid; EGTA, ethylene glycol bis($\beta$-aminoethyl ether)-*N*,*N*,*N*′,*N*′-tetraacetic acid; MLCK, myosin light chain kinase; MOPS, 3-(*N*-morpholino)propanesulfonic acid; NMR, nuclear magnetic resonance; $R_g$, radius of gyration; $R_v$, radius of gyration at infinite contrast; $I_0$, forward scattering intensity; SDS, sodium dodecyl sulfate; Tris, tris(hydroxymethyl)aminomethane.

scattering angle and λ the wavelength of the incident radiation] before being combined (Seeger & Pynn, 1986; Hjelm, 1987, 1988). Wavelength-dependent transmission corrections, background subtraction, and spectral normalization are applied during this combination. All data are recorded and archived in full three-dimensional histograms, allowing compromises between resolution and count rate to be made during data reduction rather than during data acquisition.

When proper corrections are made, the scattering probability is a function only of $Q$ and not of neutron wavelength. Each time slice provides data over a range of $Q$ which is limited by the beam stop and the detector radius. We have further limited the lowest $Q$ data for three reasons: for a molecule as small as calmodulin, the lowest $Q$ regime is not required in the analysis, the subtraction of background near the beam stop is imprecise for biological samples because they scatter neutrons weakly; and the possibility of data contamination in the lowest $Q$ regime by inelastic downscatter of shorter wavelength neutrons by water in the sample has not been eliminated (Hjelm, 1988). The reduced data from the LQD are usually presented as a dimensionless scattering probability, $(N/A)\mathrm{d}\sum(Q)/\mathrm{d}\Omega$, where $N/A$ is the number of scattering particles per unit area of sample and $\mathrm{d}\sum(Q)/\mathrm{d}\Omega$ is the differential coherent scattering cross section per scatterer. Division of this quantity by the sample thickness gives the neutron intensity: $I(Q) = (N/V)\mathrm{d}\sum(Q)/\mathrm{d}\Omega$ in units of $\mathrm{cm}^{-1}$, where $V$ is the volume of the scattering particle. There is some uncertainty in the absolute calibration of $I(Q)$, but relative values are well determined as indicated by the quoted statistical errors.

*Data Analysis.* Radius of gyration, $R_g$, and forward scatter, $I_0$, were initially determined by using a Guinier analysis (Guinier, 1939). Subsequently, the scattering data were analyzed by using the indirect Fourier-transform method as parameterized by Moore (1980). The functions $QI(Q)$ and $P(r)/r$, where $P(r)$ is the distribution of chord lengths in the molecule, are a Fourier-transform pair. The model consists of setting $P(r)/r$ to zero at $r = 0$ and above a maximum vector length $d_{max}$ and representing it as a series of sine functions between $r = 0$ and $r = d_{max}$ [the value of $d_{max}$ is determined from the $P(r)$ fitting procedure (see below)]. The truncated sine functions become differences of $\sin(x)/x$ functions when transformed to reciprocal space (in which the data are collected). The number of terms, $n$, in the series is limited by $d_{max}Q_{max}/\pi$, where $Q_{max}$ is the maximum $Q$ of the experiment. The neutron data for calmodulin allowed four terms to be determined. The smaller $d_{max}$ value for calmodulin complexed with MLCK-I allowed only three terms to be determined for the neutron data, which (along with $d_{max}$) represent the total information content of the data. The X-ray experiments generally measured to higher $Q$ values than the neutron experiments, allowing extra terms (usually one or two) to be determined. In addition, the X-ray experiments used a slit-shaped source, and so the $\sin(x)/x$ functions were further modified by integrating over slit width and height. The LQD has pinhole geometry, so a new version of Moore's program was written which averages the basis functions over the actual bin widths (not necessarily equal) of the experimental $I(Q)$ function.

The great advantage of the indirect transform method is that once the coefficients of the basis functions have been found by fitting to the scattering data, the $P(r)/r$ curve is immediately defined by the same coefficients applied to the sine functions in real space. The zeroth and second moments of $P(r)$ can be integrated analytically to find $I_0$ and $R_g$, respectively. Furthermore, the covariance matrix of the coefficients is well-defined, and the statistical precision of any derived quantity [in particular, $I_0$, $R_g$, and the $P(r)$ function itself] is easily calculated. It is much more difficult to estimate the inaccuracy of the model resulting from the limited number of terms determined in the series (or equivalently, from the limited range of $Q$). If one assumes that $I(Q) \propto Q^{-4}$ for $Q > Q_{max}$ (Porod, 1951), then additional terms may be estimated for $n > n_{max}$. Comparison of the $P(r)$ curves with and without the extrapolation is one way to represent the series termination error. It should be noted that the Moore code always includes this extrapolation by modifying the last basis function. This extrapolation has the danger of biasing the $P(r)$ function toward more symmetric distributions. The neutron data do not always extend to a region where $Q^{-4}$ proportionality is established; this extrapolation is not used in the analysis of the neutron data, except for estimating accuracy.

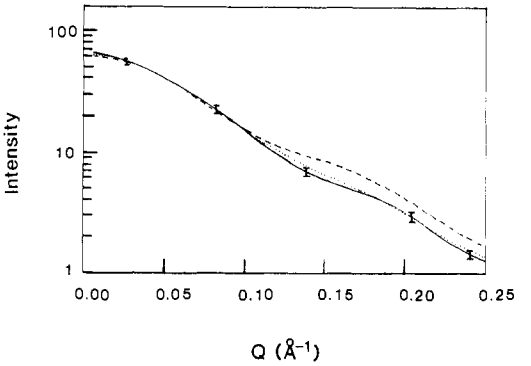


FIGURE 1: X-ray scattering intensity (in arbitrary units) as a function of $Q$ for b-CaM in the presence of $Ca^{2+}$. The solid line represents a best fit to the experimental data; the dashed and dotted lines are the profiles predicted by the crystal structures and the model derived to fit the experimental curves in Heidorn and Trewhella (1988), respectively. The model was derived from the crystal structure by allowing for conformational flexibility in the interconnecting helix region such that the globular domains are closer together, on average, by about 10 Å. Representative statistical errors are shown on the line representing the experimental data.

X-ray data were analyzed by using the original Moore code as described previously (Heidorn & Trewhella, 1988). Since the X-ray data extend to higher $Q$ than the neutron data, the measured scattering data more closely approach the $Q^{-4}$ regime. This reduces the uncertainty introduced by the extrapolation. An earlier publication (Heidorn & Trewhella, 1988) showed $P(r)$ curves derived from small-angle X-ray scattering data of calmodulin and troponin C, calculated by using the Moore code, compared with those predicted by the crystal structures of the two proteins. Differences in the $P(r)$ curves were used as a guide for modifying the crystal structures to obtain better agreement in $P(r)$ space. The same comparison has since been made in scattering space. Figure 1 shows the experimental scattering curve for calmodulin with the scattering profiles predicted by the crystal structure of calmodulin and by a model in which the two globular domains were brought closer together by allowing for flexibility in the interconnecting helix region. This comparison completely supports the conclusions drawn previously from the $P(r)$ curves and shows that differences in the models correspond to significant differences in the scattering data, and are not due to artifacts of the transformations.

Another potential problem with the $P(r)$ transformation is that the parameters $d_{max}$ and $Q_{min}$ are "soft"; i.e., there is not a good a priori way to determine them. For the neutron data presented here, Moore's procedure was used for determining $d_{max}$, i.e., choosing the minimum value which gives a good fit

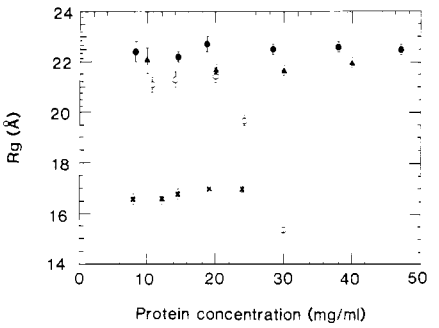


FIGURE 2: Concentration dependence of $R_g$ for c-CaM with $Ca^{2+}$ (●) and without $Ca^{2+}$ (○); deuterated c-CaM with $Ca^{2+}$ (▲); c-CaM with MLCK-I and $Ca^{2+}$ (×).

to the data and also keeps $P(r)$ positive at $r \leq d_{max}$. The minimum $Q$ value, $Q_{min}$, was then chosen to be half of the value of the first node of the basis functions. The $I_0$ and $R_g$ determined from the $P(r)$ functions for various solvent contrasts are then self-consistent, as will be shown below.

The information content of a single neutron scattering measurement is limited, but further parameters may be deduced by employing contrast variation. The $R_g$ values determined for the complex in solvents with different mean scattering densities can be interpreted by using a Stuhrmann analysis (Ibel & Stuhrmann, 1975). This analysis uses the series expansion $R_g^2 = R_v^2 + \alpha/\rho - \beta/\rho^2$, where $\rho$ is the contrast of the scattering particle with respect to the solvent and is calculated as $\rho = \bar{\rho} - \rho_s$ where $\bar{\rho}$ is the mean scattering density of the particle and $\rho_s$ the scattering density of the solvent. The coefficients $\alpha$ and $\beta$ are related to the internal density fluctuations of the particle. The coefficient $\alpha$ is the first moment of density fluctuations about the mean and is therefore related to the radial change of scattering density as a function of distance from the center of mass. Thus, for a scattering particle consisting of two subunits with different mean scattering densities, a positive $\alpha$ indicates the higher scattering density is located more toward the outside of the particle, and a negative $\alpha$ indicates it is located more toward the inside. The coefficient $\beta$ gives a measure of the separation of the centers of mass of the two scattering densities. $R_v$ is the radius of gyration of the particle at infinite contrast for which internal density fluctuations within the scattering particle are insignificant.

## Results

*X-ray Scattering.* Figure 2 shows the concentration dependence of the radius of gyration, $R_g$, for the X-ray experiments. Interparticle interference effects can give rise to quite strong concentration effects on the value of $R_g$ determined from small-angle scattering. The value of $R_g$ relevant to the actual particle shape is that calculated for infinite dilution. Unlike previously published $R_g$ data for b-CaM (Heidorn & Trewhella, 1988), the c-CaM data show no significant concentration dependence over the range 10–50 mg/mL, except for c-CaM in the absence of $Ca^{2+}$, which shows a dramatic reduction in $R_g$ for concentrations greater than 20 mg/mL. The differences in concentration dependence between c-CaM and b-CaM cannot be attributed to aggregation effects. The intensity of the forward scatter, $I_0$, is directly proportional to the molecular weight of the scattering species (Levinson et al., 1983). Plots of $I_0/c$ vs $c$ (where $c$ is the protein concentration) were linear over the entire concentration range, and the values of $I_0$ extrapolated to infinite dilution indicated each calmodulin species had the molecular weight appropriate for the soluble monomer (monodisperse lysozyme was used as a standard).

Table I: $R_g$ and $d_{max}$ Values from $P(r)$ Analyses of X-ray Scattering Data Extrapolated to Infinite Dilution

| | with $Ca^{2+}$ | | without $Ca^{2+}$ | |
|---|---|---|---|---|
| | $R_g$ (Å) | $d_{max}$ (Å) | $R_g$ (Å) | $d_{max}$ (Å) |
| b-CaM[a] | 21.3 ± 0.2 | 63 | 19.6 ± 0.12 | 59 |
| c-CaM (proteated) | 22.3 ± 0.2 | 72 | 20.5 ± 0.80 | 68 |
| c-CaM (deuterated) | 21.3 ± 0.4 | 67 | | |
| c-CaM (deuterated) + MLCK-I | 16.4 ± 0.2 | 49 | 19.8 ± 0.30 | 59 |

[a] The data for b-CaM are from Heidorn and Trewhella (1988).

The differences in concentration effects may be due to differences in charge distributions between the two forms of the protein that give rise to differences in interparticle interference effects. Differences in charge distributions may arise from the fact that the purification methods for the two species were quite different and/or from the fact that c-CaM does not have the posttranslational modifications that mammalian calmodulin has (i.e., the N-terminal acetylation and trimethylation of lysine-115). The c-CaM without $Ca^{2+}$ is the most highly charged species of calmodulin studied, and this may explain its anomalous behavior at high concentrations. In the region of 10–20 mg/mL, however, there is no significant concentration dependence for c-CaM in the absence of $Ca^{2+}$, and hence the extrapolation to infinite dilution for this species was based only on data from samples which were less than 20 mg/mL.

Table I shows the $R_g$ and $d_{max}$ values extrapolated to infinite dilution for b-CaM, for proteated (i.e., nondeuterated) c-CaM and for deuterated c-CaM with and without MLCK-I, in the presence and absence of $Ca^{2+}$. The $R_g$ values determined from the $P(r)$ analysis are in good agreement with those determined from Guinier analysis. The $R_g$ and $d_{max}$ values for the proteated c-CaM are somewhat larger (by about 5% and 15%, respectively) than those determined for b-CaM. However, the same relative increase in $R_g$ and $d_{max}$ is observed on $Ca^{2+}$ binding for c-CaM and for b-CaM. Further, the $P(r)$ curves (not shown) for the c-CaM are very similar to those published previously for b-CaM (Heidorn & Trewhella, 1988). Likewise, the $P(r)$ difference curve calculated between the $Ca^{2+}$-bound and $Ca^{2+}$-free states for c-CaM indicates an increase in vectors greater than 40 Å and a corresponding decrease in vectors below 40 Å when $Ca^{2+}$ binds. In the presence of $Ca^{2+}$, deuterated c-CaM is indistinguishable from b-CaM on the basis of a comparison of $R_g$ and $d_{max}$ values (Table I) and $P(r)$ curves (Figure 2). Within the limitations of the X-ray experiment, therefore, the deuterated bacterial calmodulin (c-CaM) and proteated bovine calmodulin (b-CaM) are equivalent in size and shape, as well as response to $Ca^{2+}$ binding. These results are consistent with the fact that bacterial "wild type" calmodulins are indistinguishable from bovine calmodulin in target enzyme activation assays (Putkey et al., 1986; Persechini et al., 1989).

When MLCK-I is added to deuterated c-CaM in the presence of $Ca^{2+}$, calmodulin undergoes a dramatic conformational rearrangement, as evidenced by a decrease in $R_g$ of 4.9 Å and a decrease in the maximum linear dimension ($d_{max}$) of 18 Å (Table I). The $R_g$ values for the complex do not show any significant variation over the concentration range 10–40 mg/mL (Figure 2). The $P(r)$ curve for the complex is more symmetric than that of uncomplexed c-CaM and indicates a more compact structure than uncomplexed c-CaM (Figure 3). X-ray data obtained using b-CaM plus MLCK-I show the same structural changes as with c-CaM and peptide. When MLCK-I is added to CaM in the absence of $Ca^{2+}$, no change in calmodulin structure is observed; the $R_g$ value for b-CaM

Table II: Parameters Derived from Guinier and $P(r)$ Analyses of the Neutron Scattering Data

| | | Guinier | | $P(r)$ | | | | |
|---|---|---|---|---|---|---|---|---|
| | % $D_2O$ | $R_g$ (Å) | $I_0$ ($cm^{-1}$) | $R_g$ (Å) | $I_0$ ($cm^{-1}$) | $d_{max}$ (Å) | $\chi^2$ | df[a] |
| c-CaM (deuterated) with $Ca^{2+}$ | 0 | 18.5 ± 0.2 | 0.948 ± 0.005 | 19.4 ± 0.2 | 0.965 ± 0.006 | 59 | 80.2 | 91 |
| c-CaM (deuterated) with MLCK-I and $Ca^{2+}$ | 0 | 14.6 ± 0.15 | 0.827 ± 0.004 | 15.1 ± 0.2 | 0.846 ± 0.005 | 45 | 61.1 | 84 |
| | 18 | 16.6 ± 0.2 | 0.571 ± 0.004 | 16.0 ± 0.2 | 0.564 ± 0.004 | 45 | 76.9 | 84 |
| | 37 | 16.4 ± 0.3 | 0.312 ± 0.003 | 16.7 ± 0.2 | 0.322 ± 0.004 | 41 | 79.5 | 80 |
| | 56 | 18.6 ± 0.9 | 0.201 ± 0.006 | 18.2 ± 0.6 | 0.199 ± 0.006 | 49 | 81.4 | 86 |
| | 75 | 17.9 ± 0.6 | 0.088 ± 0.002 | 18.0 ± 0.5 | 0.088 ± 0.002 | 53 | 89.4 | 89 |

[a] df = degrees of freedom = number of data − number of parameters.

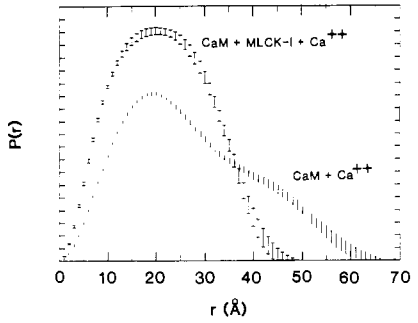


FIGURE 3: $P(r)$ curves calculated from X-ray scattering data extrapolated to infinite dilution for deuterated c-CaM and deuterated c-CaM plus MLCK-I, both in the presence of $Ca^{2+}$.

plus MLCK-I is the same as for b-CaM in the absence of MLCK-I and $Ca^{2+}$ (Table I), and the respective $P(r)$ curves show no significant differences.

*Neutron Scattering.* Figure 4 shows the contrast dependence of the neutron scattering data for the complex of deuterated c-CaM and MLCK-I (24 mg/mL total protein) in the presence of $Ca^{2+}$. Five different solvent contrasts were obtained by varying the percentage of $D_2O$ (0%, 18%, 37%, 56%, and 75%). Pure $D_2O$ was not used because the contrast of the complex with respect to the solvent would be too low to acquire meaningful data. The lines in Figure 4 represent the least-squares fits of the $P(r)$ model to the scattering data (see Data Analysis). The values of $I_0$, $R_g$, and $\chi^2$ (with the number of degrees of freedom) for these fits are given in Table II, along with the results of the Guinier analyses for the same data sets. There is very good agreement between the $R_g$ and $I_0$ values determined by using the $P(r)$ model and the Guinier analysis for the neutron scattering data. The errors shown are only propagated counting statistics; no estimate of systematic errors has been made. Statistical uncertainties for $R_g$ are generally lower when determined from $P(r)$ compared with the Guinier analysis because more data points contribute to the determination.

Neutron data were also collected from deuterated c-CaM in $H_2O$ without MLCK-I, and Figure 5 compares the $P(r)$ curve calculated for the complexed c-CaM in 37% $D_2O$ to that for the uncomplexed c-CaM in $H_2O$. Each $P(r)$ is represented by a band with half-width equal to one standard deviation, to show the statistical precision of the model fit. The neutron $P(r)$ curves are in excellent agreement with the X-ray data, showing a marked reduction of $R_g$ and $d_{max}$ for calmodulin when it binds the MLCK-I peptide (see also Table II). This conformational change is reflected in the $P(r)$ curves and in $R_g$ and $d_{max}$ values for all of the different contrasts measured for the complex (Table II). The $P(r)$ curves for the complex in 37% $D_2O$ are shown because at this contrast the MLCK-I peptide is very close to its solvent match point (as calculated from its chemical composition); thus, the peptide does not contribute significantly to the scattering. The $P(r)$ curve obtained under these conditions, therefore, most closely represents vectors from calmodulin alone. The dashed lines in Figure 5 show the effect of appending a $Q^{-4}$ extrapolation to the fitted $I(Q)$ curves. For the complex, which gives a nearly symmetric $P(r)$ function, there is very little difference between the $P(r)$ function calculated with or without the extrapolation. In the case of the uncomplexed calmodulin, which has a more elongated structure, as evidenced by a more asymmetric $P(r)$ function, the differences between the curves calculated with and without the $Q^{-4}$ extrapolation are significant and indicate the limits of the accuracy of the model. The $P(r)$ transfor-

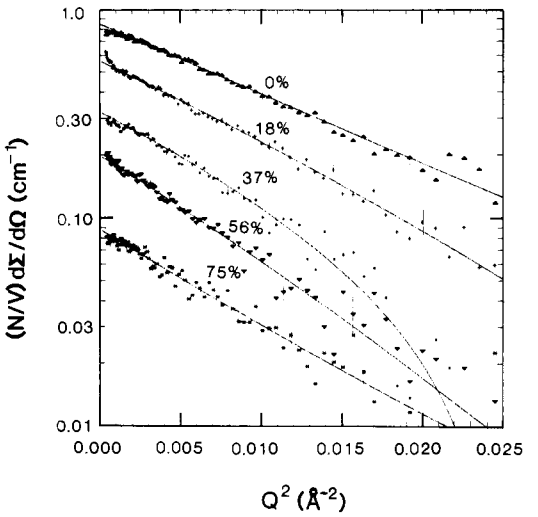


FIGURE 4: Neutron scattering data for c-CaM (deuterated) plus MLCK-I in the presence of $Ca^{2+}$. All samples were 24 mg/mL, with deuterated CaM and proteated MLCK-I. Contrast was varied by changing the $D_2O$:$H_2O$ ratio in the solvent; the percentages indicated represent the percentage of $D_2O$. The data are shown on a Guinier plot, but the lines are least-squares fits of the Moore $P(r)$ model. Representative error bars are shown.

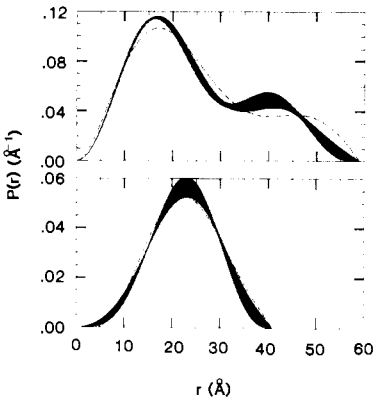


FIGURE 5: Fitted length distribution functions for deuterated c-CaM in $H_2O$ (top) and for the complex of deuterated c-CaM with proteated MLCK-I with $Ca^{2+}$ in 37% $D_2O$. The band representing each $P(r)$ is ±1 standard deviation in height, indicating propagated statistical errors, and the dashed lines show the effect of extrapolating the data as $Q^{-4}$.

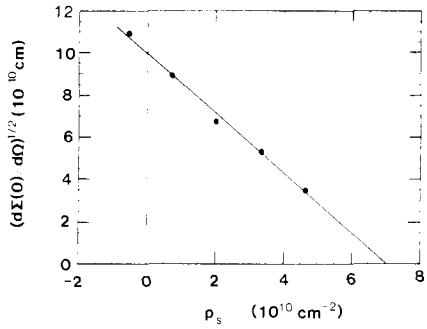


FIGURE 6: Dependence of the neutron forward scatter for deuterated c-CaM complexed with proteated MLCK-I (in the presence of $Ca^{2+}$) on the solvent scattering density.

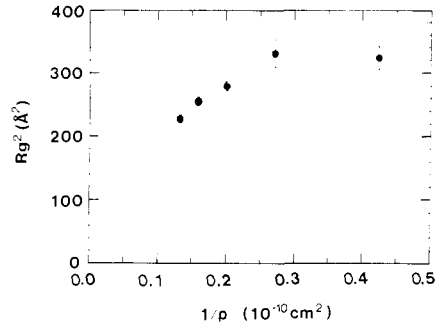


FIGURE 7: $R_g^2$ versus $1/\rho$ (Stuhrmann plot) for deuterated c-CaM complexed with proteated MLCK-I in the presence of $Ca^{2+}$; $\rho = \bar{\rho} - \rho_s$, where $\bar{\rho}$ is the mean scattering density of the complex and $\rho_s$ the solvent scattering density.

mations for both uncomplexed and complexed CaM, however, are in excellent qualitative agreement with each other and with the results of the X-ray analysis.

A direct comparison of the values of $R_g$ and $d_{max}$ for similar samples obtained from X-ray and neutron experiments reveals differences in the absolute values of as much as 10%. For example, the X-ray-determined $R_g$ for deuterated c-CaM with $Ca^{2+}$ is 21.3 Å, compared to a value of 19.6 Å for the $R_g$ of the same sample measured by using neutrons. This difference is not inconsistent with the inherent differences for X-ray and neutrons in contrast between the particle and the solvent, and in scattering density fluctuations within the scattering particle. There may also be a contribution from uncertainty in the absolute calibration of the neutron spectrometer. However, the observed conformational changes and reduction of $R_g$, as well as the contrast dependence of $R_g$, are independent of the absolute calibration.

The contrast dependence of the square root of the forward scattering cross section per particle is shown in Figure 6. These values were determined by dividing the $I_0$ values in Table II by the number of molecules per unit volume, which is the same for all samples. As expected, the dependence is linear. The extrapolated intercept on the contrast axis gives a mean scattering density, $\bar{\rho}$, for the complex of $7.0 \times 10^{-10}$ cm$^2$. This gives an estimate of the particle volume, $V_p$, for the complex of 22 000 Å$^3$ (using $\bar{\rho} = \sum b_i / V_p$, where $\sum b_i$ is the sum of the scattering lengths of the atoms in the particle). This agrees very well with the value of 23 340 Å$^3$ estimated from the partial specific volume (0.72 cm$^3$/g) and molecular weight (19 600) for the proteated complex. Note that the volume determined using $\bar{\rho}$ corresponds to the unhydrated volume of the particle and is expected to be somewhat smaller than the hydrated volume of the complex.

Figure 7 shows $R_g^2$ plotted as a function of $1/\rho$ (a Stuhrmann plot) for the neutron data from the complex. In principle, it is possible to fit these data to a quadratic equation and determine values for $\alpha$, $\beta$, and $R_v$ (see Data Analysis); however, the errors in the parameters derived by this method for these data are very large, and extrapolation to infinite contrast is not statistically significant. Our interpretation of the Stuhrmann analysis is therefore confined to the fact that the data are consistent with a quadratic whose maximum lies on the positive side of the $R_g^2$ axis. Hence, $\alpha$ is positive, indicating that the higher scattering density component (the deuterated molecule of c-CaM) is located more toward the outside of the particle and the lower scattering density component (the proteated molecule of MLCK-I) is located more toward the inside of the particle. The curvature of the Stuhrmann plot suggests that the centers of mass of the peptide and the calmodulin are not coincident. To determine the parameters quantitatively requires data at negative contrast, i.e., proteated calmodulin complexed with deuterated MLCK-I. Deuterated MLCK-I was not available for these experiments.

## Discussion

Molecular details of the solution structure of calmodulin complexed with other molecules such as peptides and target enzymes are very limited at present. Although previous studies have shown that MLCK-I binding to calmodulin appears to induce an $\alpha$-helical structure in the peptide, and that calmodulin undergoes global structural changes as the result of complex formation (Klevit et al., 1985), the size and shape of the complex, as well as the relative dispositions of the peptide and calmodulin in the complex, are as yet unknown. The combined use of small-angle X-ray and neutron scattering to study the complex of calmodulin and MLCK-I peptide has provided valuable insights regarding the solution structural properties of the complex.

When MLCK-I binds to calmodulin, a dramatic conformational rearrangement takes place that is reflected by reductions both in the radius of gyration ($R_g$) and in the maximum dimension ($d_{max}$) of the complex. These data indicate that MLCK-I peptide binding causes calmodulin to contract into a significantly more compact structure. The length distribution function, $P(r)$, for the deuterated c-CaM–MLCK-I complex at the solvent match point for the peptide indicates that on binding MLCK-I calmodulin adopts a very compact structure such that its mass is distributed more toward its center of mass as compared with the dumbbell-shaped uncomplexed calmodulin. Further, if it is assumed that the overall structures of the two globular domains of uncomplexed calmodulin remain relatively unchanged, then the maximum linear dimension for calmodulin when complexed with MLCK-I (41 Å) indicates that the globular domains must form close contacts [the globular domains are described in the crystal structure as ellipsoids with approximate dimensions of 20 × 20 × 25 Å (Babu et al., 1985)]. The $P(r)$ function derived from the X-ray data, to which the peptide and protein contribute equally, indicate that the complex as a whole also has a compact structure. Both the X-ray and neutron experiments give a reduction of the dimensions of the complex of approximately 20% compared with uncomplexed calmodulin.

Neutron scattering data experiments performed using a set of solutions having a range of scattering densities (i.e., different $D_2O$:$H_2O$ ratios) can provide information concerning the relative disposition of the components in a complex if the components have different scattering densities (i.e., if one component is deuterated and one proteated). This information can be quantified by using the Stuhrmann analysis (see Data Analysis). This analysis works best when data are measured

on either side of the mean scattering density of the complex (i.e., at positive and negative contrast), thus allowing the determination of the radius of gyration at infinite contrast, $R_v$, by interpolation rather than by extrapolation. Determination of $R_v$ by extrapolation, as in this case, results in large uncertainties. Likewise, the coefficients $\alpha$ and $\beta$ which give information on the radial distribution of scattering density within the particle are poorly determined. In this experiment, the mean scattering density for the complex is at a value that exceeds the scattering density for pure $D_2O$. It was therefore not possible to measure even one data point on the other side of the $1/(\bar{\rho} - \rho_s)$ axis, and thus interpretation of the Sturhmann plot is limited to qualitative statements. The Stuhrmann analysis indicates that the deuterated calmodulin is distributed more toward the outside of the complex and the MLCK-I peptide is localized more toward the inside and that the centers of mass of the two components are not coincident.

No significant conformational change is observed for calmodulin if MLCK-I is added in the absence of $Ca^{2+}$. This is not unexpected and is consistent with complex formation and MLCK activation being $Ca^{2+}$ dependent. Previous CD measurements (Klevit et al., 1985) which showed a dramatic increase in $\alpha$-helix content for a mixture of calmodulin and MLCK-I in the presence of $Ca^{2+}$ likewise showed a minimal increase in helix content in the absence of $Ca^{2+}$. Similarly, NMR experiments (Klevit et al., 1985) that showed widespread spectral changes for calmodulin on complexing MLCK-I showed little effect in the absence of $Ca^{2+}$.

A number of calmodulin–peptide interactions have been studied by a variety of techiques, and it appears that there is a broad range of structural possibilities depending on the properties of the peptide sequence. The peptides melittin and mastoparan both bind to calmodulin with high affinity and have been used by a number of investigators as models to study calmodulin–peptide interactions. Recent time-resolved fluorescence anisotropy studies of photo-cross-linked calmodulin complexed with melittin and with mastoparan indicate only modest changes in the overall structure of calmodulin (Small & Anderson, 1988) that appear inconsistent with the type of global conformational rearrangement evidenced in the small-angle scattering data when calmodulin binds MLCK-I. Proton NMR studies comparing various calmodulin–peptide interactions (Klevit & Blumenthal, 1987) have also indicated that MLCK-I induces more extensive structural changes in calmodulin than either melittin or mastoparan. The physiological significance of these differences between various peptide–calmodulin complexes is not clear, but further comparison of different calmodulin–peptide interactions may provide important clues to the basis for calmodulin's ability to activate different target enzymes.

The finding that calmodulin undergoes a large conformational change involving a dramatic contraction on binding the MLCK peptide indicates that there is considerable flexibility in the solvent-exposed central helix. This flexibility is likely important for target enzyme interactions and may be essential for calmodulin to interact with such a wide variety of target enzymes. Evidence for flexibility in the central helix was suggested by the crystal structure data (Babu et al., 1988) and was also indicated in earlier solution X-ray studies from this laboratory (Heidorn & Trewhella, 1988), as well as studies using genetically engineered calmodulin mutants (Persechini & Kretsinger, 1988; Persechini et al., 1989; Putkey et al., 1988). The significant contraction in the structure of calmodulin upon binding the MLCK peptide also suggests that the peptide interacts directly with both lobes of calmodulin in the complex. This conclusion is supported by recent fluorescence binding data showing that the MLCK peptide binds with 10000-fold lower affinity to either the N-terminal or the C-terminal half-fragments of calmodulin generated by trypsin digestion (Blumenthal and Klevit, unpublished observation).

One concern in interpreting data from calmodulin–peptide interactions in terms of target enzyme activation mechanisms is that the larger target enzyme may impose constraints on the interaction that could substantially change the structural response in calmodulin. While there are data to suggest these peptides are useful models and there are compelling technical limitations that have led to focusing on the peptide interactions, it remains important to work toward a more physiological system. We are currently working on experiments that will hopefully allow us to eventually study calmodulin interactions with either larger target enzyme fragments or whole target enzymes using neutron scattering and contrast variation techniques.

## Acknowledgments

We thank Rachel Klevit for discussions and suggestions that led to these experiments. We also thank Theresa Honeycutt for her excellent technical assistance in the preparation and characterization of synthetic peptides. We thank Rex Hjelm for helpful discussions on the analysis of the neutron data.

## References

Babu, Y. S., Sack, J. S., Greenhough, T. C., Bugg, C. E., Means, A. R., & Cook, W. J. (1985) *Nature 315*, 37.

Babu, Y. S., Bugg, C. E., & Cook, W. J. (1988) *J. Mol. Biol. 204*, 191.

Blumenthal, D. K., & Krebs, E. G. (1987) *Methods Enzymol. 139*, 115.

Blumenthal, D. K., & Krebs, E. G. (1988) in *Molecular Aspects of Cellular Regulation* (Cohen, P., Klee, C. B., Eds.) Vol. 5, pp 341–356, Elsevier, Amsterdam.

Blumenthal, D. K., Takio, K., Edelman, A. M., Charbonneau, H., Titani, K., Walsh, K. A., & Krebs, E. G. (1985) *Proc. Natl. Acad. Sci. U.S.A. 82*, 3187.

Guinier, A. (1939) *Ann. Phys. (Paris) 12*, 161.

Hanley, R. M., Means, A. R., Ono, T., Colbran, R. J., Kemp, B. E., Soderling, T. R., & Means, A. R. (1987) *J. Biol. Chem. 263*, 7190.

Heidorn, D. B., & Trewhella, J. (1988) *Biochemistry 27*, 909.

Hjelm, R. P. (1987) *J. Appl. Crystallogr. 20*, 273.

Hjelm, R. P. (1988) *J. Appl. Crystallogr. 21*, 618.

Ibel, K., & Stuhrmann, H. B. (1975) *J. Mol. Biol. 93*, 255.

Kemp, B. E., Pearson, R. B., Guerriero, V., Bagchi, I. C., & Means, A. R. (1987) *J. Biol. Chem. 262*, 2542.

Klevit, R. E., & Blumenthal, D. K. (1987) in *Proceedings of the 5th International Symposium on Calcium Binding Proteins in Health and Disease*, pp 333–347, Academic Press, New York.

Klevit, R. E., Blumenthal, D. K., Wemmer, D. E., & Krebs, E. G. (1985) *Biochemistry 24*, 8152.

LaPorte, D. C., Wierman, B. C., & Storm, D. R. (1980) *Biochemistry 19*, 3814.

Levinson, B. L., Pickover, C. A., & Richards, F. M. (1983) *J. Biol. Chem. 258*, 10967.

Moore, P. B. (1980) *J. Appl. Crystallogr. 13*, 168.

Nunnally, M. H., Blumenthal, D. K., Krebs, E. G., & Stull, J. T. (1987) *Biochemistry 26*, 5885.

Payne, M. E., Fong, Y.-L., Ono, T., Colbran, R. J., Kemp, B. E., Soderling, T. R., & Means, A. R. (1988) *J. Biol. Chem. 263*, 7190.

Persechini, A., & Kretsinger, R. H. (1988) *J. Biol. Chem. 263*, 12175.
Persechini, A., Blumenthal, D. K., Jarett, H. W., Klee, C. B., Hardy, D. O., & Kretsinger, R. H. (1989) *J. Biol. Chem.* (in press).
Porod, G. (1951) *Kolloid-Z. 124*, 83.
Putkey, J. A., Draetta, G. F., Slaughter, G. R., Klee, C. B., Stull, J. T., & Means, A. R. (1986) *J. Biol. Chem. 261*, 9896.
Putkey, J. A., Ono, T., VanBerkum, M. F. A., & Means, A. R. (1988) *J. Biol. Chem. 263*, 11242.
Seeger, P. A., & Pynn, R. (1986) *Nucl. Instrum. Methods Phys. Res., Sect. A 424*, 115.
Seeger, P. A., Williams, A., & Trewhella, J. (1987) in *Proceedings of the International Collaboration on Advanced Neutron Sources-IX* (Atchison, F., & Fischer, W., Eds.) SIN Report ISBN 3-907990-01-4, p 437, Swiss Institute for Nuclear Research, Villigen, Switzerland.
Seeger, P. A., Hjelm, R. P., & Nutter, M. J. (1989) *Mol. Cryst. Liq. Cryst.* (in press).
Seeholzer, S. H., Cohn, M., Putkey, J. A., Means, A. R., & Crespi, H. L. (1986) *Proc. Natl. Acad. Sci. U.S.A. 83*, 3634.
Small, E., & Anderson, S. R. (1988) *Biochemistry 27*, 419.
Stull, J. T. (1988) in *Molecular Aspects of Cellular Regulation* (Cohen, P., Klee, C. B., Eds.) Vol. 5, pp 91-119, Elsevier, Amsterdam.
Tanaka, T., & Hidaka, H. (1980) *J. Biol. Chem. 255*, 11078.
Wylie, D. C., & Vanaman, T. C. (1988) in *Moleclar Aspects of Cellular Regulation* (Cohen, P., Klee, C. B., Eds.) Vol. 5, pp 1-15, Elsevier, Amsterdam.

# Postulated Role of Calsequestrin in the Regulation of Calcium Release from Sarcoplasmic Reticulum†

Noriaki Ikemoto,*,‡,§ Michel Ronjat,‡,∥ László G. Mészáros,‡,⊥ and Makoto Koshita‡,#

*Department of Muscle Research, Boston Biomedical Research Institute, Boston, Massachusetts 02114, and Department of Neurology, Harvard Medical School, Boston, Massachusetts 02115*

*Received November 22, 1988; Revised Manuscript Received May 2, 1989*

ABSTRACT: $Ca^{2+}$ release from heavy sarcoplasmic reticulum (SR) vesicles was induced by 2 mM caffeine, and the amount ($A$) and the rate constant ($k$) of $Ca^{2+}$ release were investigated as a function of the extent of $Ca^{2+}$ loading. Under both passive and active loading conditions, the $A$ value increased monotonically in parallel to $Ca^{2+}$ loading. On the other hand, $k$ sharply increased at partial $Ca^{2+}$ loading, and upon further loading, it decreased to a lower level. Since most of the intravesicular calcium appears to be bound to calsequestrin both under passive and under active loading conditions, these results suggest that the kinetic properties of induced $Ca^{2+}$ release show significant variation depending upon how much calcium has been bound to calsequestrin at the time of the induction of $Ca^{2+}$ release. An SR membrane segment consisting of the junctional face membrane (jfm) and attached calsequestrin (jfm–calsequestrin complex) was prepared. The covalently reacting thiol-specific conformational probe *N*-[7-(dimethylamino)-4-methyl-3-coumarinyl]maleimide (DACM) was incorporated into several proteins of the jfm, but not into calsequestrin. The fluorescence intensity of DACM increased with $Ca^{2+}$. Upon dissociation of calsequestrin from the jfm by salt treatment, the DACM fluorescence change was abolished, while upon reassociation of calsequestrin by dilution of the salt it was partially restored. These results suggest that the events occurring in the jfm proteins are mediated via the attached calsequestrin rather than by a direct effect of $Ca^{2+}$ on the jfm proteins. We propose that the [$Ca^{2+}$]-dependent conformational changes of calsequestrin affect the jfm proteins and in turn regulate the $Ca^{2+}$ channel functions.

Calsequestrin is one of the major protein components of the sarcoplasmic reticulum (SR),[1] but its physiological role has not yet been thoroughly understood. During the nearly 2 decades since its discovery (MacLennan & Wong, 1971; Ikemoto et al., 1971), extensive studies have been carried out on its physicochemical properties (MacLennan et al., 1983; Campbell, 1986). The isolated calsequestrin molecule in solution is presumably in a monomeric form (Ikemoto et al., 1974; Hymel et al., 1984) with an asymmetric structure (Cozens & Reithmeier, 1984). The isolated protein is highly acidic (MacLennan & Wong, 1971; Ikemoto et al., 1974; MacLennan et al., 1983; Campbell, 1986; Fliegel et al., 1987; Scott et al., 1988) and has characteristic $Ca^{2+}$ binding properties (MacLennan & Wong, 1971; Meissner et al., 1973; Ikemoto et al., 1974; Slupsky et al., 1987) with a large capacity

† This work was supported by Grant AR-16922 from the National Institutes of Health and by a grant from the Muscular Dystrophy Association of America.

* Address correspondence to this author at the Department of Muscle Research, Boston Biomedical Research Institute, 20 Staniford St., Boston, MA 02114.
‡ Boston Biomedical Research Institute.
§ Harvard Medical School.
∥ Permanent address: Laboratoire de Biophysique Moleculaire et Cellulaire, Centre d'Etudes Nucleaires, Grenoble 38041, France.
⊥ Present address: Second Institute of Biochemistry, Semmelweis University Medical School, Budapest, Hungary.
# Present address: Department of Physiology, Nagoya City University Medical School, Nagoya, Japan.

[1] Abbreviations: DACM, *N*-[7-(dimethylamino)-4-methyl-3-coumarinyl]maleimide; DTT, dithiothreitol; EGTA, ethylene glycol bis(β-aminoethyl ether)-*N*,*N*,*N*′,*N*′-tetraacetic acid; jfm, junctional face membrane; MES, 2-(*N*-morpholino)ethanesulfonic acid; SR, sarcoplasmic reticulum; T-tubule, transverse tubular system.

0006-2960/89/0428-6764$01.50/0 © 1989 American Chemical Society